Characterizing the monomer-dimer equilibrium of UbcH8/Ube2L6: A combined SAXS and NMR study

Kerem Kahraman[1], Scott A. Robson[2], Oktay Göcenler[1], Cansu D. Tozkoparan[1], Jennifer M. Klein[3], Cansu M. Yenici[1], Arthur L. Haas[3], Joshua J. Ziarek[2,], Çağdaş Dağ[1,4,]* *

[1]Nanofabrication and Nanocharacterization Center for Scientific and Technological Advanced Research (n[2]STAR), Koc University, İstanbul, Turkey

[2]Department of Molecular and Cellular Biochemistry, Indiana University, 212 S. Hawthorne Drive, Bloomington, IN 47405, USA

[3]Department of Biochemistry and Molecular Biology, LSUHSC-School of Medicine, 1901 Perdido Street, New Orleans, LA, 70112, USA

[4]Koc University Isbank Center for Infectious Diseases (KUISCID), Koc University, Istanbul, Turkey

*Corresponding author: cdag@ku.edu.tr, jjziarek@indiana.edu

KEYWORDS. ISGlyation, ubiquitination, E2 enzyme, TRACT, oligomerization

ABSTRACT: Interferon-stimulated gene-15 (ISG15) is an interferon-induced protein with two ubiquitin-like (Ubl) domains linked by a short peptide chain, and the conjugated protein of the ISGylation system. Similar to ubiquitin and other Ubls, ISG15 is ligated to its target proteins with a series of E1, E2, and E3 enzymes known as Uba7, Ube2L6/UbcH8, and HERC5, respectively. Ube2L6/UbcH8 plays a literal central role in ISGylation, underscoring it as an important drug target for boosting innate antiviral immunity. Depending on the type of conjugated protein and the ultimate target protein, E2 enzymes have been shown to function as monomers, dimers, or both. UbcH8 has been crystalized in both monomeric and dimeric forms, but the functional state is unclear. Here, we used a combined approach of small-angle X-ray scattering (SAXS) and nuclear magnetic resonance (NMR) spectroscopy to characterize UbcH8's oligomeric state in solution. SAXS revealed a dimeric UbcH8 structure that could be dissociated when fused with an N-terminal glutathione S-transferase molecule. NMR spectroscopy validated the presence of a concentration-dependent monomer-dimer equilibrium and suggested a backside dimerization interface. Chemical shift perturbation and peak intensity analysis further suggest dimer-induced conformational dynamics at ISG15 and E3 interfaces - providing hypotheses for the protein's functional mechanisms. Our study highlights the power of combining NMR and SAXS techniques in providing structural information about proteins in solution.

INTRODUCTION

Interferon-Stimulated Gene 15 (ISG15), also known as hUCRP or IP17, is a 15 kDa ubiquitin-like, type I interferon (IFN) inducible protein [1]. ISGylation is an ubiquitin-like (Ubl) post-translational modification (PTM) that involves the covalent attachment of ISG15 to target proteins [2]. Similar to other Ubls, ISGylation plays important roles in various cellular processes such as innate antiviral immunity, protein degradation, and signal transduction [3]. Free, unconjugated, ISG15 also serves immunoregulatory functions as a cytoplasmic and secreted signaling protein in eukaryotic organisms [4]. Inherited ISG15 deficiency dramatically reduces the innate immune system's ability to fight viruses in mice yet only appears to cause immunoregulatory issues against mycobacterial, not viral diseases, in humans [3]. Thus, the role of ISG15 in human viral pathogenesis is not clearly understood.

The ISGylation cascade requires the sequential action of three enzymes: Ube1L as the E1 enzyme, UbcH8 as the E2 enzyme, and HERC5 as the E3 enzyme. First, ISG15 binds the catalytically active cysteine of the Ube1L activating enzyme (E1) in an ATP-dependent reaction. Then, E1 interacts with UbcH8 conjugating enzyme (E2) through its ubiquitin folding domain (UFD), which facilitates the transesterification of active ISG15, and results in an intermediate ISG15-UbcH8 complex joined by a thioester bond [5]. Finally, HERC5 ligase enzyme (E3) interacts with the intermediate ISG15-UbcH8 complex to mediate ligation of ISG15 to the target protein. UbcH8 plays a central role in ISGylation as it interacts with both E1 and E3 enzymes - making it a key target for the regulation of the ISGylation pathway [6].

Under reducing conditions, E2 enzymes can spontaneously form dimers when a crosslinker is added [7], and apart from a few exceptions, E2 enzymes are capable of preserving their dimer form [8, 9]. Nevertheless, both the dimer and the monomer forms of E2 enzymes are capable of recruiting E3 enzymes and conjugating ubiquitin [10]. Although dimeric E2 enzymes are perceived as more advantageous because one of the monomers can remain associated while the ubiquitin conjugation continues with the other.

The Protein DataBank (PDB) contains both dimeric (PDB ID:1WZV) and monomeric (PDB ID:1WZW) crystal structures of UbcH8. Yet, it is unknown whether UbcH8 dimerizes naturally or as a consequence of non-specific crystal packing contacts. In this study, we aimed to characterize the oligomeric state of human UbcH8 (Ube2L6) in solution using Small Angle X-ray Scattering (SAXS). We first used a fusion protein approach with the goal of producing a high-resolution scattering envelope to properly place the UbcH8 protomers. Surprisingly, UbcH8 formed stable dimers upon removal of the N-terminal fusion protein. We next used solution nuclear magnetic resonance (NMR) spectroscopy to first validate and then further characterize the monomer-dimer equilibrium. Our results indicate that UbcH8 contains a substantial dimer population at 150 μM concentration and that dimerization may induce conformational changes at the distal ISG and E3 interaction interfaces.

RESULTS

GST fusion guides SAXS protein structural modeling. To determine the state of UbcH8 in solution, we expressed and purified it fused to an N-terminal glutathione-S transferase (GST) tag herein termed GST-UbcH8. We hypothesized that the 28 kDa GST molecule should be easily

discernible from the smaller (18 kDa) UbcH8, and would dramatically improve fitting SAXS scattering data to the structural model. The sample was concentrated to 280 μM and six, 10 min SAXS frames were collected for a total of one hour. Superimposition of each 10 min frame confirmed that the X-ray beam produced little to no detectable radiation damage (data not shown). The medium to high q region, which is emphasized in the q vs l(q) plot, is consistent with a folded sample (Figure 1A). The Kratky plot possessed a bell-shaped curve that approaches zero after reaching a maximum at ~3 sRg; this result is consistent with a properly folded, globular protein (Figure 1B). While slight deviations between the typical Kratky plot and dimensionless Kratky plot can aid in the assessments of flexibility, no apparent differences were observed.

The pair-distance distribution function, P(r), is a measure of the frequency of interatomic distances that can also provide information about the protein shape. The presence of a shoulder in the P(r) suggests a multidomain protein as expected for the GST-UbcH8 fusion (Figure 1C). The largest distance (D_{max}) in the P(r) histogram was 8 nm (Figure 1C). The GST-UbcH8 crystal structures were then fitted into the final 3D DAMMIF dummy atom model (Figure 1D,E). Both GST and UbcH8 proteins, as well as the linker peptide, are clearly visible fitting a monomeric model. The fact that even the linker region can be detected with SAXS analysis and be observed this clearly, underscores the power of SAXS in structure determination. After GST cleavage, UbcH8 was observed to form a dimer based on Size Exclusion Chromatography (data not shown), hence we hypothesized that GST mayblock the dimerization site.

FreeUbcH8 is a Dimer in Solution. To test how well the GST-fusion improves the modeling of UbcH8 into the SAXS scattering, we prepared a second UbcH8 sample with the GST protein

removed. Again, we concentrated UbcH8 to 280 μM and collected six, 10 min frames for a total of 1 h (Figure 2A). Similar to GST-UbcH8, the Kratky plot possessed a bell-shaped curve that approaches zero (Figure 2B). We estimated a slightly larger R_g ~ 4.40 nm, compared to GST-UbcH8, from the low q region, whereas the P(r) D_{max} was reduced to 6.2 nm (Figure 2C). Surprisingly, the free UbcH8 P(r) also contained a shoulder suggesting homodimerization (Figure 2C). ATSAS molecular weight analysis predicts a 39.5 kDa particle, which is approximately double the expected 18 kDa UbcH8. We then fitted the UbcH8 dimer crystal structure (PDB 1WZV; Figure 2D) to the dummy atom model the scattering envelope (Figure 2E). The best-fit model (X^2 = 1.7) possesses a dimerization interface with the active site cysteines of each protomer pointed outwards (Figure 2D,E). The consistency between the previously published dimer crystal structure and the dummy atom model obtained by SAXS analysis, supports the homodimer formation of UbcH8 protein in solution in absence of a GST-tag.

NMR analysis of UbcH8 monomer-dimer equilibrium. To further establish dimerization of UbcH8 in solution, we performed Transverse Relaxation Optimized Spectroscopy (TROSY) for rotational correlation times (TRACT) experiments [11,12] to estimate the rotational correlation time (τ_c) of UbcH8 at two different concentrations: 300 μM and 150 μM (Figure 3). The signal intensity ranging from 8.6 to 9.2 ppm was integrated to maximize signal to noise and emphasize well-structured regions of the protein that are representative of global tumbling. We estimated ^{15}N relaxation rates for the TROSY and anti-TROSY integrated signals using Bayesian Parameter Estimation of a two-parameter single-exponential decay model. This method produces a distribution of decay rates, which encompass uncertainty, that were then used to determine the cross-correlated relaxation (CCR) rate. The rotational correlation time was estimated from CCR

according to an algebraic solution [12] of the modified Goldman relation [13], assuming an order parameter (O^2) of 0.8. We determined a τ_c ~16 ns at 300 μM and ~13 ns at 150 μM (Figure 3), which demonstrates a concentration dependence on molecular rotation diffusion times. We then used hydroNMR [14] to model rotational diffusion of monomeric and dimeric UbcH8 from the PDB 1WZV dimeric crystal structure. hydroNMR reported a τ_c = 20.5 ns for the dimer and 7.4 ns for the monomer at 25 ºC. Taken together, this confirms that UbcH8 undergoes monomer-dimer exchange and indicates a substantial dimer population even at 150 μM. Data could not be collected at lower concentrations due to the sensitivity limit of the room temperature NMR probe.

We next collected ^{15}N heteronuclear single quantum coherence (HSQC) solution NMR spectra at 150 μM and 300 μM to identify UbcH8's dimerization interface. Resonances were assigned by visual inspection using BMRB Entry ID 16321 as a reference list. The NH resonances of all residues except for the 18 prolines were assigned (79.85% completion). We then assessed both concentration-dependent chemical shift perturbations (CSPs) and peak intensity differences. The concentration-dependent CSPs were of relatively low magnitude and located far from the crystallographic dimerization interface (Figure 4). All of the perturbed residues except for N23, which resides at the dimerization site, are situated at either the E1 or the ISG15 interaction surfaces. Residues E80, N81, and G82 are clustered on a loop near the catalytic C85 residue where ISG15 is covalently attached. Whereas F56, K99, V103, L104, and N108 are proximal to the E1 binding region on the UbcH8 surface; interestingly, these residues are arranged towards the UbcH8 core rather than at the surface (Figure 4). Given that ISG15 and E1 involve distinct interfaces, we hypothesize a conformational change or allosteric pathway influences the transfer

or binding of ISG15. Our results suggest that dimerization may play an additional role in ISGylation. We hypothesize that the weak CSPs could reflect a mostly sidechain-mediated interface and/or that the ensemble is predominantly dimeric even at 150 μM concentration.

Thus, we also measured the concentration-dependent changes in peak intensity. We hypothesize these intensity differences result from monomer-dimer exchange on the intermediate (microsecond-millisecond) timescale, but it's also possible that they reflect dimerization-dependent fluctuations in longitudinal (T_1) or transverse (T_2) relaxation. The largest changes in peak intensity again clustered to the ISG15 and E1 interfaces, while also highlighting an extended region along the crystalized dimer interface (Figure 5). D149 sits at the center of the dimerization surface with E141 and L144 in close proximity. It's plausible that D28 and A29, located in a loop region of the opposing protomer, could possess the flexibility to interact. Furthermore as the overall structure gets bigger with the dimerization, decreased signals from some peaks were expected due to line broadening. Although unlike the CSP analysis which showed that most of the conformational changes occurred away from the dimerization site, delta chemical shift intensity analysis revealed that most of the affected residues were on the dimerization site. In fact, the peak intensity of N23 and D149 residues (Supp. Figure 4) from opposing protomers, which are within 3.3 Å distance in the crystal structure, deviated from the mean peak height by 44.7% and 62.2%, at 150μM, and 37.6% and 35.6%, at 300 μM, respectively. Taken together, this indicates that dimerization is *ipso facto* involved in defining interaction dynamics between E1 and E2 enzymes.

DISCUSSION

In this study, we investigated the oligomeric state of UbcH8 in solution using Small Angle X-ray Scattering (SAXS) and NMR analysis. To improve the fitting of SAXS scattering data to the structural model, we initially employed an N-terminal GST-fused UbcH8 protein. The results from SAXS experiments and analysis indicate that the GST-UbcH8 fusion protein is monodisperse and properly folded in solution. The 3D DAMMIF dummy atom model also revealed a monomeric model of the GST-UbcH8 fusion protein, highlighting the advantages of SAXS in structure determination. The free form of UbcH8, without the GST fusion, was further investigated. Surprisingly, the P(r) distribution suggested a multidomain complex, and the ATSAS molecular weight analysis indicated dimer formation. The consistency between the existing crystal structure of UbcH8 dimer and the SAXS-derived dummy atom model supports the formation of a UbcH8 homodimer in solution in the absence of a GST-tag.

Our NMR analysis, including chemical shift perturbation and peak intensity measurements, provide additional evidence for the dimerization of UbcH8. Residues involved in the dimerization process were identified, and the effects of dimerization on the E1 and ISG15 interaction sites were observed. The TRACT experiments also supported the dimerization of UbcH8, revealing a concentration-dependent behavior of UbcH8 in solution, which suggests monomer-dimer exchange on an intermediate timescale. The dimerization of UbcH8 and its implications on the ISGylation process are consistent with previous reports of E2 enzymes forming dimers to facilitate polyubiquitination [10]. Dimerization of several E2 enzymes are reported and the observed dimerization of the enzymes are found to be stimulating the catalytic activity of the E2 enzyme in these studies [9,15,16,17]. In 2010, David et. al. suggested that E2 enzymes form dimers in solution regardless if an active ubiquitin is present [7]. While the

monomer form is also active for the acquisition of the ubiquitin, dimer form of the E2 is found to be more advantageous as while one monomer site is binding the ubiquitin molecules, the other site is capable of remaining associated to the target protein and thus facilitates efficient polyubiquitination. The acting mechanism of E2 enzymes proposed in this study suggests that the E2 enzymes function as dimers while catalyzing polyubiquitination process [7]. Our results demonstrate that UbcH8, the E2 enzyme specific for ISGylation, can also form dimers at near physiological concentrations. This suggests that the ISGylation process may also involve dimerization for regulating the complicated interactions of E1, E2 and E3 enzymes. This study highlights the importance of understanding the oligomeric state and behavior of proteins in solution to gain insights into their biological function and regulation. Moreover, our work emphasizes the usefulness of SAXS and NMR techniques in elucidating protein structures and interactions in solution, which can complement crystallographic studies and provide a more biologically relevant context.

Future studies may focus on exploring the functional implications of UbcH8 dimerization in the ISGylation process, such as the effects on substrate specificity, E1 and E3 enzyme interactions, and the kinetics of ISGylation. Additionally, the molecular mechanisms underlying the observed concentration-dependent behavior of UbcH8 and the role of post-translational modifications in modulating its oligomeric state could be investigated further. These studies will contribute to a more comprehensive understanding of the regulation and function of UbcH8 in the context of ISGylation and its broader implications in various diseases, including viral and bacterial infections, cancer, and autoimmune disorders.

MATERIALS AND METHODS

Protein expression and purification. Three alanine residues followed by the coding sequence of the UbcH8 protein are inserted in the 5' BamH1/ 3' EcoR1 restriction sites of the pGEX-4T3 plasmid. Three alanine residues are inserted between the GST and UbcH8 protein sequence in order to increase the binding efficiency and also to provide a better cleavage upon thrombin treatment during the purification of the protein sample. The final coded amino acid sequence was:MSPILGYWKIKGLVQPTRLLLEYLEEKYEEHLYERDEGDKWRNKKFELMGLEFPNL PYYIDGDVKLTQSMAIIRYIADKHNMLGGCPKERAEISMLEGAVLDIRYGVSRIAYSKDFE TLKVDFLSKLPEMLKMFEDRLCHKTYLNGDHVTHPDFMLYDALDVVLYMDPMCLDAF PKLVCFKKRIEAIPQIDKYLKSSKYIAWPLQGWQAFGGGDHPPKSDLVPRGSAAAMASM RVVKELEDLQKKPPPYLRNLSSDDANVLVWHALLLPDQPPYHLKAFNLRISFPPEYPFKP PMIKFTTKIYHPNVDENGQICLPIISSENWKPCTKTCQVLEALNVLVNRPNIREPLRMDLA DLLTQNPELFRKNAEEFTLRFGVDRPS*

pGEX-4T3 GST-AAA-UbcH8 plasmid was transformed into Rosetta2 *E. Coli* expression cells, plated on LB-ampicillin-chloramphenicol, and grown overnight at 37 °C. The next morning, colonies were picked from the agar plate and inoculated into 10 ml LB-ampicillin-chloramphenicol medium. The culture was grown overnight at 37 °C at 110 rpm. The overnight culture was transferred into 1 L LB medium and incubated at 37°C. After OD_{595} exceeded 0.3, temperature was lowered to 18°C and protein production was induced at OD_{595} 0.8 by the addition of 0.4mM IPTG. Cells were harvested 18 hours after induction by centrifugation at 2000 RCF for 1 hour.

Harvested cells were resuspended in lysis buffer (500mM NaCl, 50mM Tris, 0.1% (v/v) Triton X-100, 5% (v/v) glycerol, 1mM DTT, pH=7.5), sonicated, and centrifuged at 20K RCF for 1 hour to remove insoluble debris. The obtained supernatant was loaded to a GST affinity column equilibrated with 20mM Tris (pH 7.5), 150mM NaCl, 1mM DTT. Non-specific proteins were washed with the same buffer and the protein was eluted with 30mM glutathione, 20mM Tris (pH 7.5), 150mM NaCl, 1mM DTT. For cleavage of the GST tag, 1:100 thrombin enzyme was added to the eluted protein and dialyzed in 20mM Tris (pH 7.5), 150mM NaCl, 1mM DTT solution overnight to eliminate excess glutathione. For separation of the GST tag, reverse GST chromatography was applied. Unbound free UbcH8 was collected and purified by size exclusion chromatography using 20mM Tris (pH 7.5), 150mM NaCl, 1mM DTT buffer.

SAXS Data Collection. All SAXS data were collected at home source SAXSpoint 5.0 (Anton Paar GmbH) as described before [18]. Sample/detector distance (SDD) was 1600 mm for SAXS experiments. All measurements took place at 10 °C. Data was collected in one hour session(1-minutes long 6 frames) for each measurement. The scattering curves were checked for radiation damage and no damage was detected after the superimposition of each 10 minute data collection intervals..

SAXS Data Processing and Modeling. At first, the scattering pattern of all samples were visually inspected in the Primus program of ATSAS 3.0 for any possible issues with the measurement[11]. The radius of gyration (Rg) was calculated using Guinier's equation and inverse Fourier transform by Primus. Distance distribution function P(r) and the maximum

particle diameter (Dmax) was calculated by GNOM[19]. After estimating the molecular weight of the model DAMMIF (ab initio) is used to generate 5 independent low resolution models from the data. [20]. DAMAVER and DAMMIN then averaged, clustered, and optimized these 5 distinct solutions to form the final ab-initio shape [21]. SASpy plug-in for PyMOL was used to superimpose the homology modeled structure of the protein [22, 23].

^{15}N Labeled Protein Expression and Purification. pGEX-4T3 GST-AAA-UbcH8 plasmid containing bacteria were grown overnight in LB medium at 37°C and transferred into 50 mL ^{15}N labeled M9 media the next day. Following 4 hours of incubation at 37°C, cells were transferred into 1L M9 media. After OD_{595} exceeded 0.3, temperature was lowered to 18°C and protein production was induced at OD_{595} 0.8 by the addition of 0.4mM IPTG. The medium contained 33.7mM Na_2HPO_4, 22 mM KH_2PO_4, 8.55 mM NaCl, 9.35 mM ^{15}N labeled NH_4Cl, 1mM $MgCl_2$, 0.3mM $CaCl_2$, and 7 mg/L $FeCl_2$-$4H_2O$. Cells were harvested 18 hours after induction by centrifugation at 2000 RCF for 1 hour.

Harvested cells were resuspended in lysis buffer (500mM NaCl, 50mM Tris, 0.1% (v/v) Triton X-100, 5% (v/v) glycerol, 1mM DTT, pH=7.5), sonicated, and centrifuged at 20K RCF for 1 hour to remove insoluble debris. The obtained supernatant was loaded to a GST affinity column equilibrated with 38.39 mM Na_2HPO_4, 11.61 mM KH_2PO_4 (pH 7.4), 100 mM NaCl, 1mM DTT. Non-specific proteins were washed with the same buffer and the protein was eluted with 30mM glutathione, 38.39 mM Na_2HPO_4, 11.61 mM KH_2PO_4 (pH 7.4), 100 mM NaCl, 1mM DTT. For cleavage of the GST tag, 1:100 thrombin enzyme was added to the eluted protein and dialyzed in 38.39 mM Na_2HPO_4, 11.61 mM KH_2PO_4 (pH 7.4), 100 mM NaCl, 1mM DTT solution overnight to eliminate excess glutathione. For separation of the GST tag, reverse GST chromatography was

applied. Unbound free UbcH8 was collected and purified by size exclusion chromatography using 38.39 mM Na_2HPO_4, 11.61 mM KH_2PO_4 (pH 7.4), 100 mM NaCl, 1mM DTT buffer.

NMR Data Acquisition and analysis. The protein was concentrated to 0.287 mM. 10% D2O (final concentration) containing 1mM DSS was added to obtain a final sample volume of 600 µL. All NMR data acquisition process was completed using 500 MHz Bruker Ascend magnet equipped with Avance NEO console and BBO double resonance room temperature probe at Koç University n^2STAR NMR Facility. 2-D ^{1}H-^{15}N HSQC spectra were recorded with 50% non-uniform sampling (NUS) at 298 K with a 1H spectral width of 14 ppm (1024 data points in t2) and a ^{15}N spectral width of 32 ppm (64 data points in t1). The 2D data was processed by NMRPipe [24] and analyzed using NMRFAM-SPARKY [25]. The combined ^{1}H-^{15}N chemical shift perturbations were calculated using equation $\Delta\delta_{AV} = [(\Delta\delta\ ^{1}H)^2 + (\Delta\delta\ ^{15}N*0.14)^2]^{1/2}$ [26].

1D TRACT experiments [11] were collected with 1024 complex points and 1.5 s recycle delay. Relaxation rates for ^{15}N TROSY and anti-TROSY components were determined from spectra intensity values integrated over 9.2 to 8.6 ppm at eight relaxation delays: 30, 60, 90, 120, 150, 180, 210, 240, 270 and 300 ms. Each relaxation rate and its uncertainty was estimated by fitting the integrated values and time delays to a single parameter exponential decay model using Bayesian Parameter Estimation. Each TROSY and anti-TROSY relaxation rate was then used to estimate rotational correlation time (τ_c) using the algebraic method [12] where we assumed an order parameter (O^2) of 0.8.

Author Contributions

The manuscript was written through contributions of all authors. All authors have given approval to the final version of the manuscript. CD, JJZ and ALH designed the experiments, JMK created the constructs and optimized the expression and purification; KK, OG expressed and purified the proteins for SAXS; CMY collected SAXS data; OG, CMY and CDT analyzed SAXS data; KK, OG and CDT expressed and purified the proteins for NMR; CD, JJZ, and SAR collected the NMR data; KK and SAR processed and analyzed NMR data; CD, OG, CMY and JJZ wrote the first draft.

ACKNOWLEDGMENT

CD acknowledges support from TUBITAK (Project No: 120Z594, 122Z747). JJZ acknowledges support from National Institutes of Health grant R35GM143054. The authors acknowledge the use of the services and facilities of n^2STAR-Koç University Nanofabrication and Nanocharacterization Center for Scientific and Technological Advanced Research.

REFERENCES

[1] Haas, A. L., Ahrens, P., Bright, P. M., Ankel, H. (1987) Interferon induces a 15-kilodalton protein exhibiting marked homology to ubiquitin. Journal of Biological Chemistry, 262(23), 11315-11323.

[2] Loeb, K. R., Haas, A. L. (1992) The interferon-inducible 15-kDa ubiquitin homolog conjugates to intracellular proteins. Journal of Biological Chemistry, 267(11), 7806-7813.

[3] Perng, YC., Lenschow, D.J. (2018) ISG15 in antiviral immunity and beyond. Nat Rev Microbiol 16, 423–439

[4] Swaim CD, Scott AF, Canadeo LA, Huibregtse JM. (2017) Extracellular ISG15 Signals Cytokine Secretion through the LFA-1 Integrin Receptor. Mol Cell, 68(3):581-590

[5] Durfee, L. A., Kelley, M. L., Huibregtse, J. M. (2008) The basis for selective E1-E2 interactions in the ISG15 conjugation system. Journal of Biological Chemistry, 283(35), 23895-23902.

[6] Stewart, M. D., Ritterhoff, T., Klevit, R. E., Brzovic, P. S. (2016) E2 enzymes: more than just middle men. Cell research, 26(4), 423-440.

[7] David, Y., Ziv, T., Admon, A., Navon, A. (2010) The E2 ubiquitin-conjugating enzymes direct polyubiquitination to preferred lysines. Journal of Biological Chemistry, 285(12), 8595-8604.

[8] Vittal, V., Wenzel, D. M., Brzovic, P. S., Klevit, R. E. (2013). Biochemical and structural characterization of the ubiquitin-conjugating enzyme UBE2W reveals the formation of a noncovalent homodimer. Cell biochemistry and biophysics, 67(1), 103-110.

[9] Liess, A. K., Kucerova, A., Schweimer, K., Schlesinger, D., Dybkov, O., Urlaub, H., ... & Lorenz, S. (2020) Dimerization regulates the human APC/C-associated ubiquitin-conjugating enzyme UBE2S. Science signaling, 13(654), eaba8208.

[10] Bremm, A. (2020) Hug and hold tight: Dimerization controls the turnover of the ubiquitin-conjugating enzyme UBE2S. Science Signaling, 13(654), eabd9892.

[11] Lee, D., Hilty, C., Wider, G., Wuthrich, K. (2006) Effective rotational correlation times of proteins from NMR relaxation interference. J Magn Reson 178, 72–6.

[12] Robson, S. A., Dağ, Ç. Wu, H., Ziarek, J. J. (2021) Journal of Biomolecular NMR volume 75, 293–302.

[13] Goldman, M. (1984) Interference effects in the relaxation of a pair of unlike spin-12 nuclei. Journal of Magnetic Resonance 60, 437–452.

[14] J García de la Torre, M.L Huertas, B Carrasco (2000) HYDRONMR: Prediction of NMR Relaxation of Globular Proteins from Atomic-Level Structures and Hydrodynamic Calculations, Journal of Magnetic Resonance, 147, 1.

[15] Liu, W., Shang, Y., Zeng, Y., Liu, C., Li, Y., Zhai, L., ... Li, W. (2014) Dimeric Ube2g2 simultaneously engages donor and acceptor ubiquitins to form L ys48‐linked ubiquitin chains. The EMBO journal, 33(1), 46-61.

[16] Li, W., Tu, D., Brunger, A. T., Ye, Y. (2007). A ubiquitin ligase transfers preformed polyubiquitin chains from a conjugating enzyme to a substrate. Nature, 446(7133), 333-337.

[17] Varelas, X., Ptak, C., Ellison, M. J. (2003). Cdc34 self-association is facilitated by ubiquitin thiolester formation and is required for its catalytic activity. Molecular and cellular biology, 23(15), 5388-5400.

[18] Göcenler, O. , Yenici, C. M. , Kahraman, K. , Büyükdağ, C. & Dağ, Ç. (2022). Biomolecular Solution X-Ray Scattering At n2STAR Beamline. Mugla Journal of Science and Technology , 8 (2) , 60-69

[19] Svergun, D.I. (1992) Determination of the regularization parameter in indirect-transform methods using perceptual criteria. J. Appl. Crystallogr. 25, 495-503.

[20] Franke, D., Svergun, D.I. (2009) DAMMIF, a program for rapid ab-initio shape determination in small-angle scattering. J. Appl. Cryst., 42, 342-346.

[21] D. I. Svergun, D. I. (1999) Restoring low resolution structure of biological macromolecules from solution scattering using simulated annealing. Biophys J. 2879-2886.

[22] Schrödinger, L., DeLano, W. (2020) PyMOL. Retrieved from http://www.pymol.org/pymol.

[23] Panjkovich, A., Svergun, D. I. (2016) SASpy: a PyMOL plugin for manipulation and refinement of hybrid models against small angle X-ray scattering data. Bioinformatics, 32(13), 2062-2064.

[24] Delaglio, F., Grzesiek, S., Vuister, G.W. Zhu, G., Pfeifer, J., Bax, A. (1995) J. Biomol. NMR. 6, 277-293.

[25] Lee, W., Tonelli, M., Markley, J. L. (2015) NMRFAM-SPARKY: enhanced software for biomolecular NMR spectroscopy. Bioinformatics (Oxford, England), 31(8), 1325–1327.

[26] Williamson, M. P. (2013) Using chemical shift perturbation to characterise ligand binding, Progress in Nuclear Magnetic Resonance Spectroscopy, 73, 1-16,

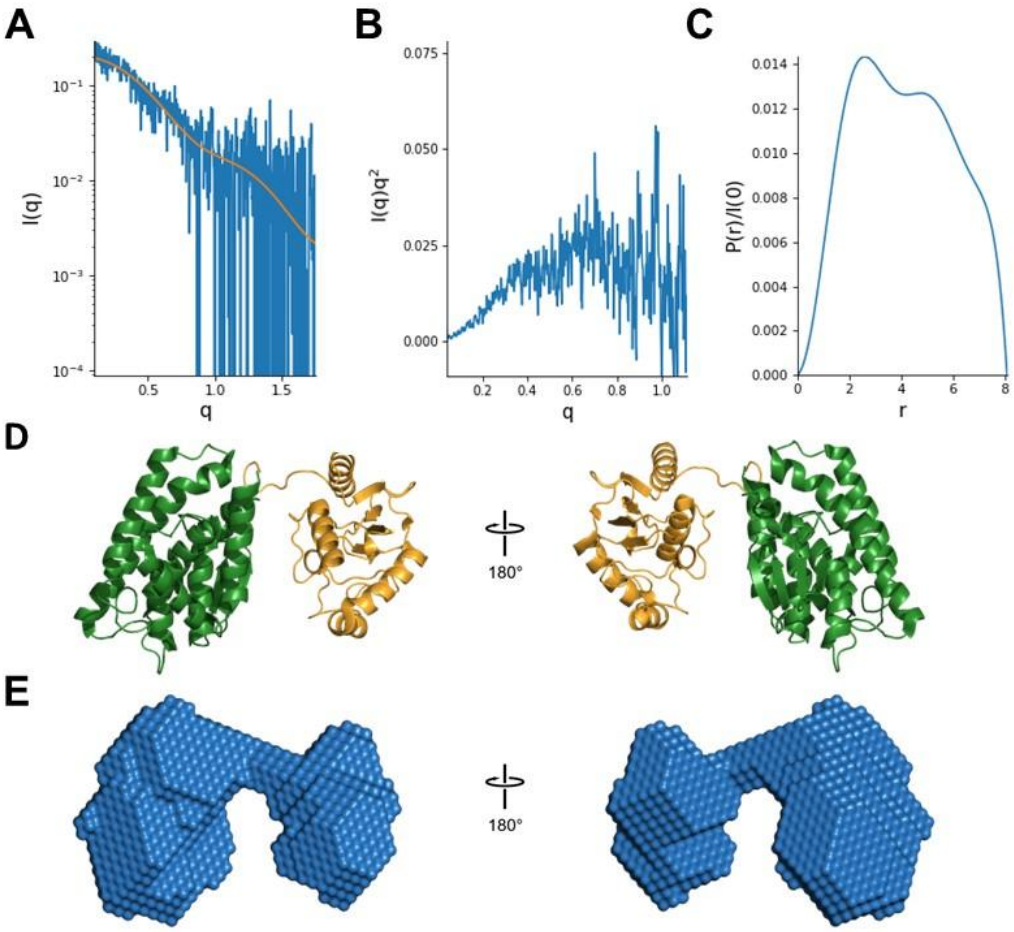

Figure 1. SAXS analysis of GST-UbcH8 fusion protein. (A) ln I (s) vs s plot, (B) Kratky plot, and (C) Pair distance distribution, P(r), plot of the experimental SAXS intensity obtained at 4.1 mg/ml (280 μM) of the GST-UbcH8 fusion protein. The pair-distance distance distribution plot of the GST-UbcH8 fusion protein scattering data calculated by GNOM. (D) The individual

crystal structures of GST (PDB:1R5A) and UbcH8 (PDB:1WZW) shown as cartoon representations. (E) The GST-UbcH8 dummy atom model, obtained by the ATSAS online package, is shown as a surface representation.

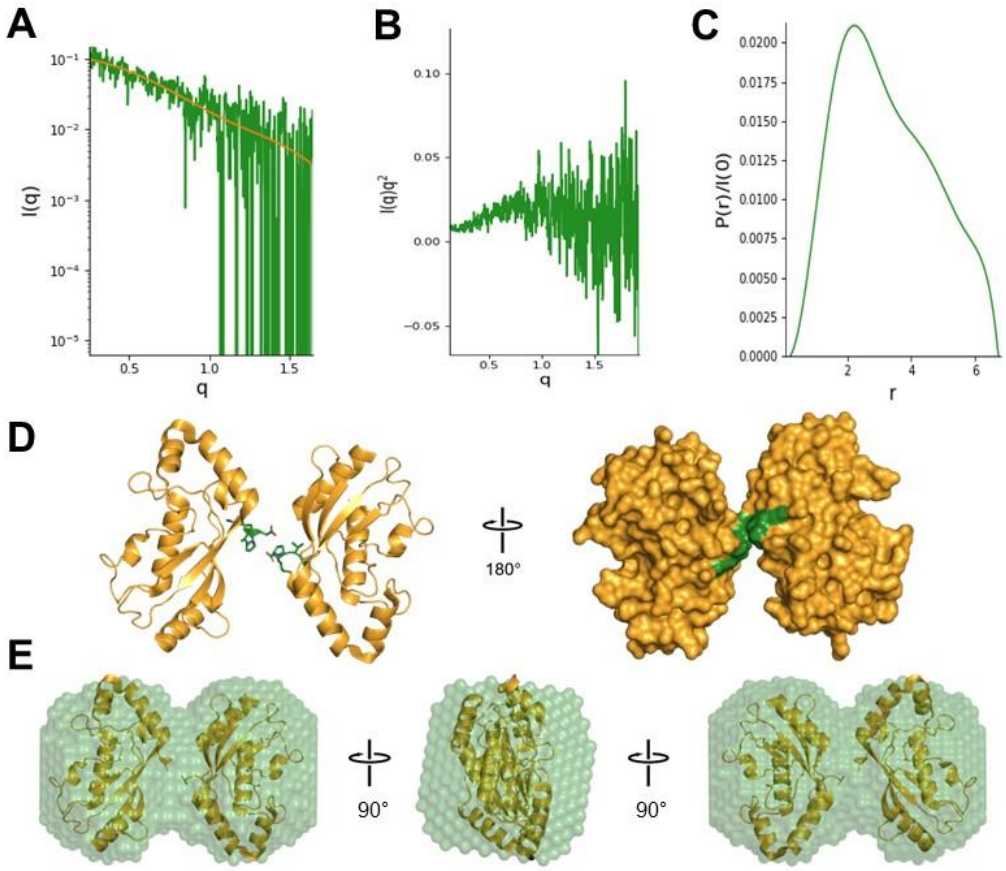

Figure 2. SAXS analysis of free UbcH8. (A) ln I (s) vs s plot, (B) Kratky plot, and (C) Pair distance distribution, P(r), plot of the experimental SAXS intensity obtained at 4.1 mg/ml (280 μM) free UbcH8 protein. (D) Crystal structure of UbcH8 dimer (pdb:1WZV) shown as cartoon and surface representation using Pymol. Residues D149, R150, and P151 of the dimerization

interface are colored forest green. (E) UbcH8 dimer crystal structure (pdb:1WZV) fitted (χ = 1.02) into the DAMMIF dummy atom model using SASpy.

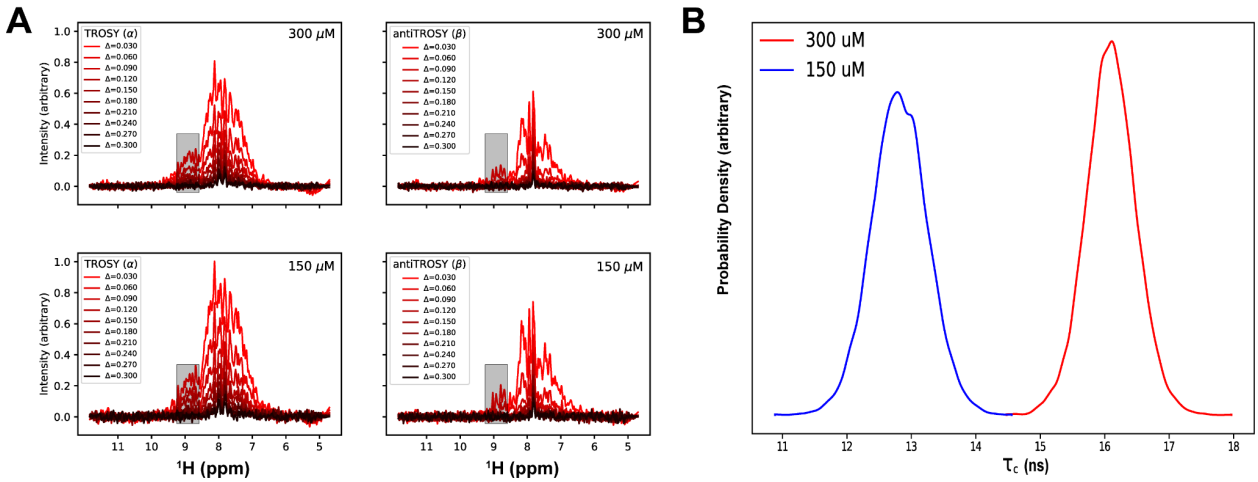

Figure 3. TRACT analysis of free UbcH8 to determine rotational correlation time. (A)The UbcH8 1D ^{15}N TROSY (left) and anti-TROSY (right) spectra from the TRACT experiment. The top and bottom panels are UbcH8 at 300 (red) and 150 μM (blue), respectively. We integrate from 8.6-9.2 ppm (gray boxed region) under the assumption that it possesses resonances from primarily structured regions. (B) The probability density estimates of the overall rotational correlation time (τ_c) for UbcH8 at 300 μM (red) and 150 μM (blue). The average (point) estimate for 300 μM and 150 μM UbcH8 are 16.1 ns and 12.8 ns, respectively.

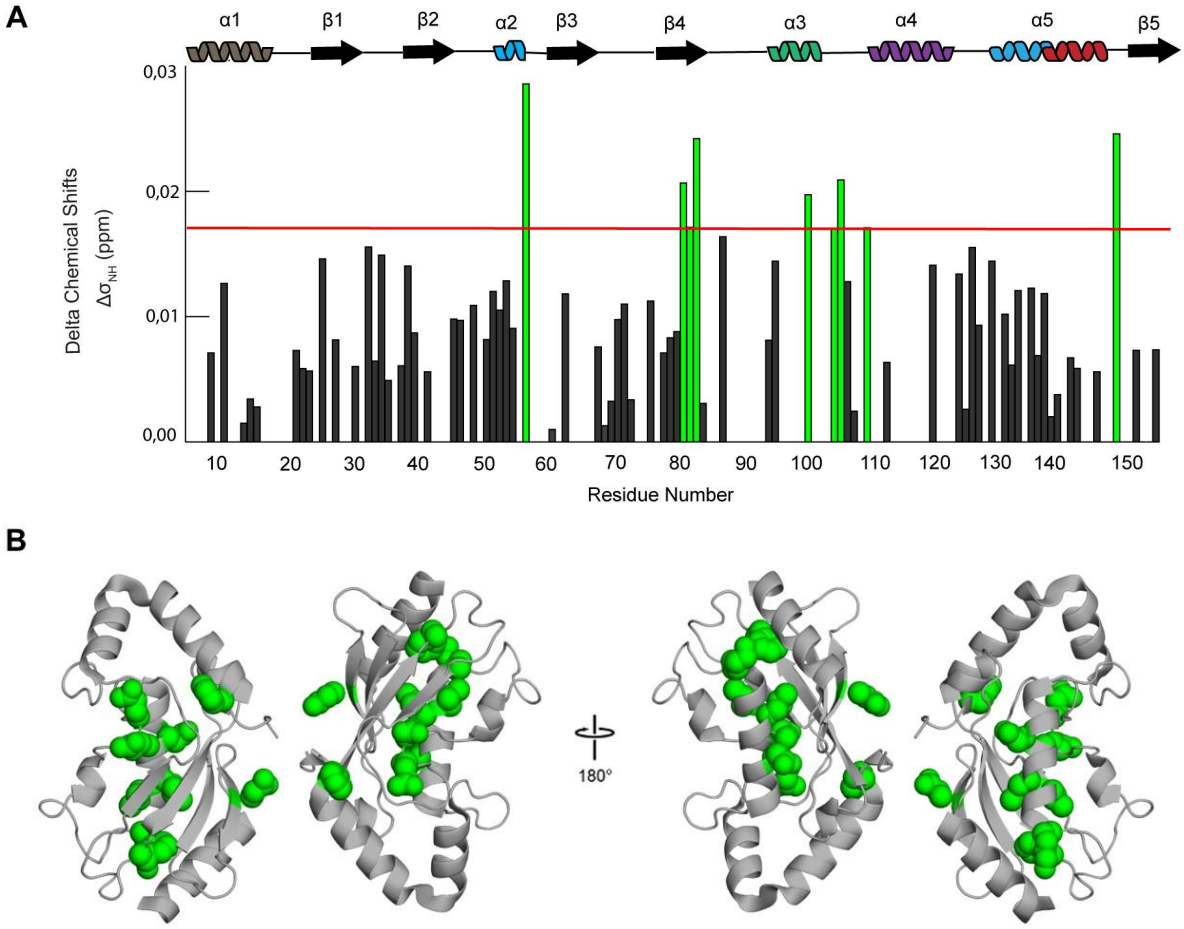

Figure 4. ^{1}H-^{15}N Chemical shift perturbations mapped onto UbcH8 dimeric crystal structure. A) The combined ^{1}H-^{15}N chemical shift perturbations between 300 μM and 150 μM UbcH8 were calculated for each residue. The residues colored green possessed chemical shift perturbations larger than the threshold (red line). Residues with no bars were not observed at either concentration. B) Residues with chemical shift perturbations larger than the threshold were mapped onto the UbcH8 dimeric crystal structure (PDB 1WZV). These residues cluster to three distinct regions: the dimer interface (N23), the ISG15 conjugation site (E80, N81, and G82), and the E1 binding surface (F56, K99, V103, L104, and N108).

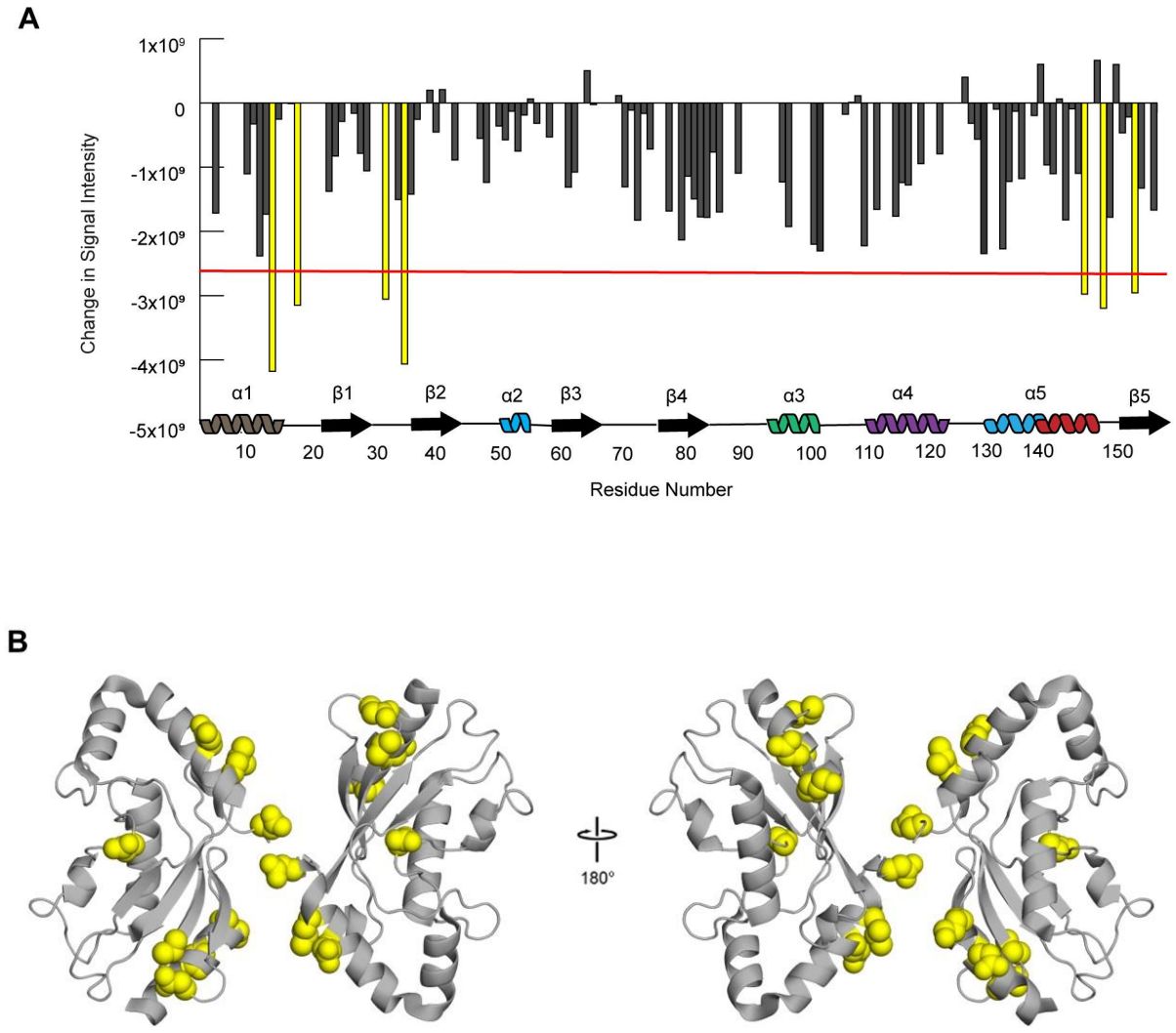

Figure 5. Concentration dependent chemical shift signal intensity changes A)Concentration-dependent changes in ^{1}H-^{15}N peak intensity mapped onto UbcH8 dimeric crystal structure. The residues colored yellow possessed peak intensity changes that were larger than the threshold (red line); these residues are D12, K16, N30, V33, E141, L144, and D149. Residues with no bars were not observed at either concentration. B) Residues with peak intensity changes larger than the threshold were mapped onto the UbcH8 dimeric crystal structure (PDB 1WZV).

SUPPLEMENTARY INFORMATION

Supplementary Table 1. Molecular Size Parameters of GST-UbcH8 and UbcH8 dimer Obtained from SAXS Data Analysis.

Sample	R_g (nm)[a]	Dmax (nm)[b]	Vp (Å^3)[c]	MW (kDa)[d]	Vc (kDa)[e]	Qp (kDa)[f]
GST-UbcH8	3.37	8	8919	41.604	41.737	42.842
UbcH8 dimer	4.402	6.2	5835	39.547	38.766	44.169

[a]Radius of gyration, [b]Maximum Dimension, [c]Porod Volume, [d]Molecular Weight, [e]Volume of Correlation, [f]Porod invariant

Supplementary Table 2. Fit quality for superimposition of E2 crystal structures onto UbcH8 dummy atom model. The UbcH8 dummy atom model was calculated from the SAXS data using DAMMIF. The fineness and normalized spatial discrepancy (NSD) of the superimposition obtained using the SASpy Pymol extension.

	3WE5	6QH3	6QHK	6S98
Fineness	1.549	1.370	1.030	1.043
Normalized Spatial Discrepancy (NSD)	2.2294	3.6498	4.9168	5.3306

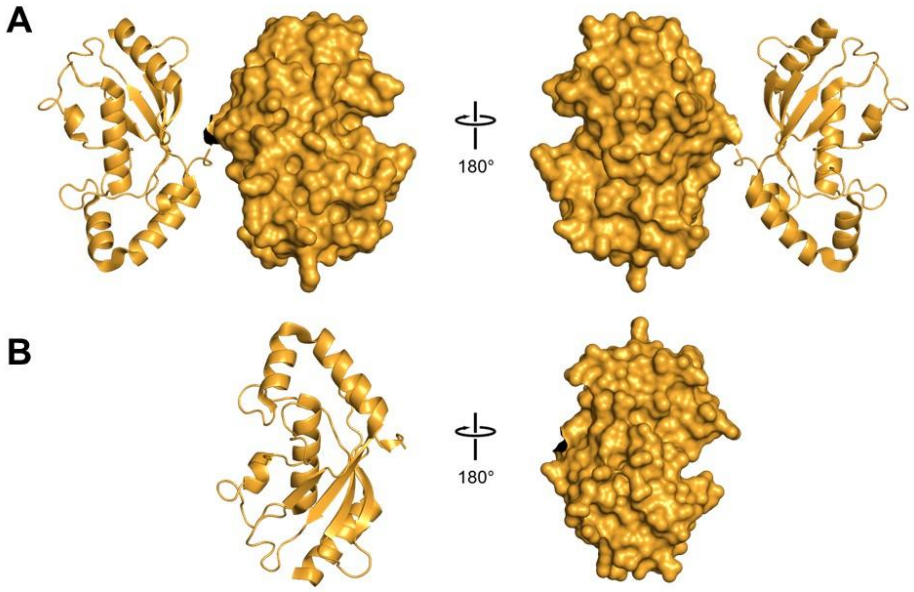

Supplementary Figure 1. Previously-determined UbcH8 crystal structures. Cartoon and surface representation of UbcH8 protein in the (A) dimeric form (PDB ID:1WZV) and (B) monomeric form (PDB ID:1WZW)

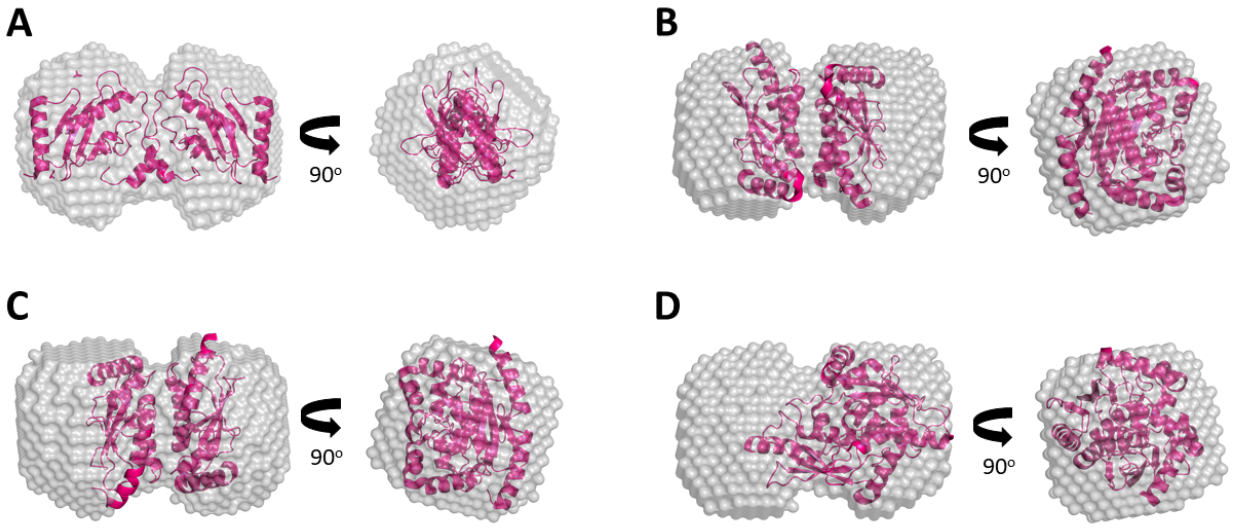

Supplementary Figure 2. Comparison of free UbcH8 dummy atom model with previously-determined E2 enzyme crystal structures. (A) Ubiquitin conjugating enzyme E2 UbcA1 from Agrocybe aegerita (PDB: 3WE5). (B) The catalytic domain of the human ubiquitin-conjugating enzyme UBE2S C118M (PDB: 6QH3). (C) The catalytic domain of the human ubiquitin-conjugating enzyme UBE2S (PDB: 6QHK). (D) The catalytic domain of wild-type UBE2S (PDB: 6S98). The free UbcH8 dummy atom model was calculated by DAMMIF.

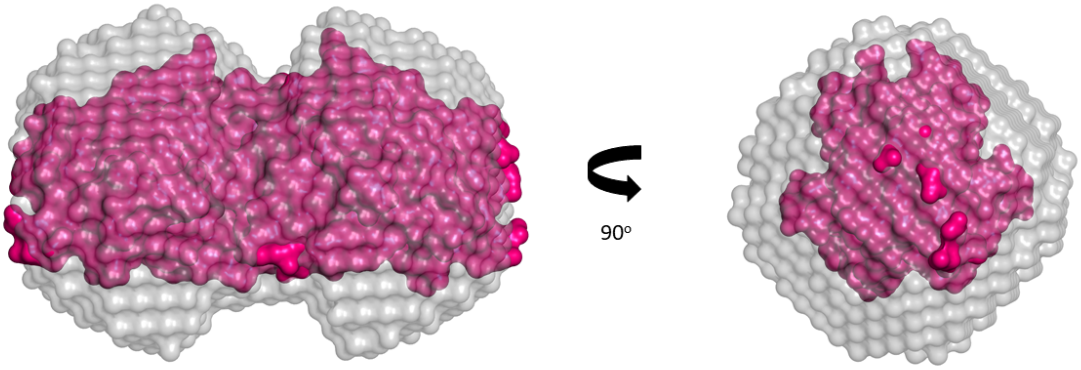

Supplementary Figure 3. Crystal structure of ubiquitin conjugating enzyme E2 UbcA1 from Agrocybe aegerita (PDB: 3WE5) shown as surface (pink) placed into the dummy model of UbcH8 dimer (Free UbcH8, gray) obtained after the DAMMIF analysis of the SAXS data, using Pymol plugin SasPY.

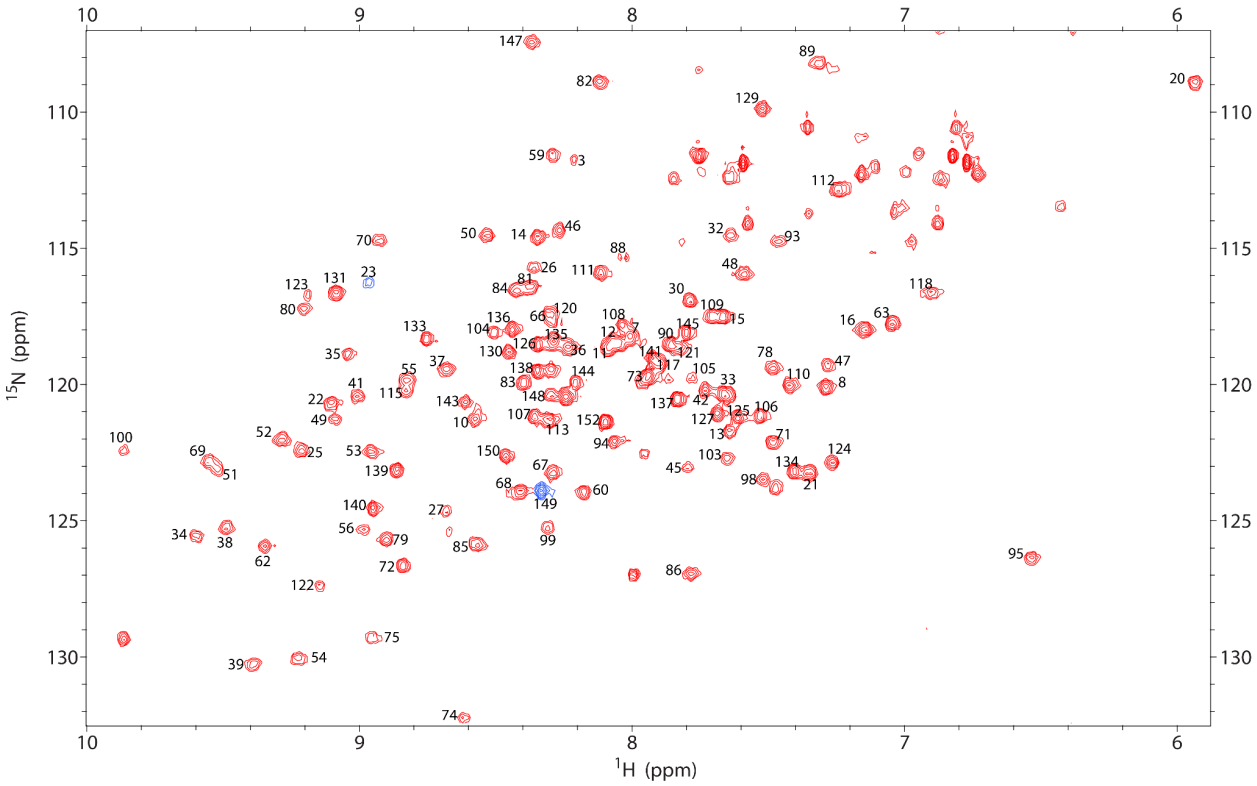

Supplementary Figure 4. ^{1}H-^{15}N HSQC spectrum of UbcH8 collected at 25°C. Residue numbers are indicated on each peak. Resonances were assigned by visual using BMRB 16321. Data were collected at 300 μM on a 11.7 T Bruker NMR spectrometer.